IEEE Photonics Journal
An IEEE Photonics Society Publication

Enhancement of Tetrahedral Chromium (Cr^{4+}) Concentration for High-Gain in Single-Mode Crystalline Core Fibers

Volume 12, Number 2, April 2020

Chun-Nien Liu, *Member, OSA*
Jhuo-Wei Li
Yung-Hsiang Tung
Chun-Chuen Yang
Wei-Chih Cheng
Sheng-Lung Huang, *Senior Member, IEEE*
Wood-Hi Cheng, *Fellow, OSA*

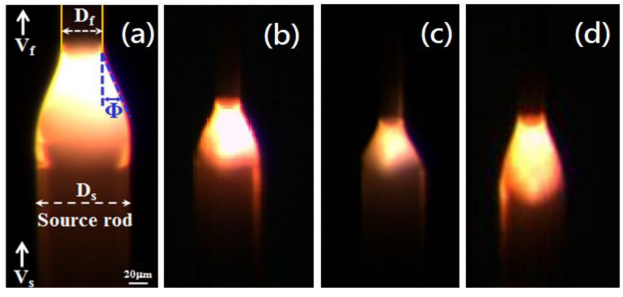

DOI: 10.1109/JPHOT.2020.2974802

Enhancement of Tetrahedral Chromium (Cr^{4+}) Concentration for High-Gain in Single-Mode Crystalline Core Fibers

Chun-Nien Liu,[1] ***Member, OSA***, **Jhuo-Wei Li**,[1] **Yung-Hsiang Tung**,[2] **Chun-Chuen Yang**,[2] **Wei-Chih Cheng**,[1] **Sheng-Lung Huang**,[3] ***Senior Member, IEEE***, **and Wood-Hi Cheng**[1] ***Fellow, OSA***

[1]Graduates Institute of Optoelectronic Engineering, National Chung Hsing University, Taichung 402, Taiwan
[2]Department of Physics, Chung Yuan Christian University, Taoyuan 320, Taiwan
[3]Graduate Institute of Photonics and Optoelectronics, National Taiwan University, Taipei 102, Taiwan

DOI:10.1109/JPHOT.2020.2974802

Manuscript received December 5, 2019; revised February 12, 2020; accepted February 13, 2020. Date of publication February 18, 2020; date of current version March 18, 2020. This work was supported by the Ministry of Science and Technology of Taiwan (MOST) under Grants 107-2221-E-005-062 and 108-2221-E-005-069-MY3. Corresponding author: Chun-Nien Liu (e-mail: terbovine@gmail.com).

Abstract: Tetrahedral chromium (Cr^{4+})-ions is the main contributor to gain in the broadband single-mode Cr-doped crystalline core fibers (SCCFs). We have demonstrated a gross gain of 8-dB on a length of 27-cm for a 300-nm broadband SCCF using a thermal annealing technique. Gross gain and fiber length are the highest yet reported for the SCCF. The record gain is mainly due to both the longer fiber by aligned molten-zone growth and Cr^{4+}-ions enhancement by thermal annealing. The enhancement mechanism of the Cr^{4+}-ions in the SCCF is experimentally verified by the means of superconducting quantum interference device (SQUID) and electron probe X-ray micro-analysis (EPMA). As a practical application of the proposed 8-dB gain in the SCCFs in fiber transmissions, a 25-Gb/s error-floor free link is successfully demonstrated.

Index Terms: Thermal annealing, fiber fabrication, fiber amplifiers, single-mode Cr-doped crystalline-core fiber.

1. Introduction

The rapidly increasing capacity of fiber transmission calls for a new generation of transport networks, including new active fibers for extended optical bandwidth. Currently, the capacity of optical transmission systems are limited to the usable gain bandwidth in rare earth-doped fiber amplifiers, which doesn't cover all the low-loss bandwidth from 1.3–1.6 μm [1]–[4]. Therefore, it is advisable to develop a fiber amplifier with broad covering of the low-loss transmitted bandwidth. Recently, Cr-doped fibers have been demonstrated the possible functions as broadband amplifiers for use in the next-generation fiber amplifiers [5]–[7]. The core material of the Cr-doped fiber was a single crystal of Cr^{4+}:YAG (chromium doped yttrium aluminum garnet) with a glass cladding. The stoichiometric formula was $[A_3][B_2](C_3)O_{12}$, where A, B, and C denoted different lattice sites with respect to their oxygen coordination that were the dodecahedral, octahedral, and tetrahedral site,

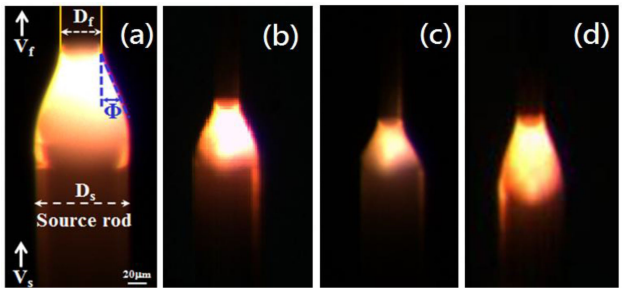

Fig. 1. (a), (b), (c), and (d) are different molten-zone shapes.

respectively [8]. The dodecahedral, octahedral, and tetrahedral sites of the Cr:YAG structure were the Y^{3+}-ions, Al^{3+}/Cr^{3+}-ions, and Al^{3+}/Cr^{4+}-ions, respectively. The Cr^{4+}(tetrahedral) ions were the major constituent of the Cr^{4+}:YAG and were used for fabricating fiber amplifiers, which emitted a broadband fluorescence of 1250–1600 nm [9]. Despite numerous studies on the Cr^{4+}(tetra)-ions enhancement in bulk materials using thermal annealing [11]–[14], limited information is available for the enhancement in fiber devices. As the Cr^{4+}(tetra)-ions enhancement may relate to gain enhancement of the fiber amplifier, therefore, it is essential for further investigation of this study to develop higher-gain fiber amplifier used in broadband fiber transmission.

In this work, the longer fiber fabrication using aligned optimization of laser-heated pedestal growth (LHPG) and the Cr^{4+}-ions enhancement employing thermal annealing technique are proposed for gain enhancement of the single-mode chromium-doped crystalline core fibers (SCCFs). A gross gain of 8-dB on a fiber length of 27-cm for a 300-nm broadband SCCF using a thermal annealing technique is demonstrated. In comparison with previous reports [7], [15], this study has improved in the fiber length and gain performance of the SCCFs. The 8-dB gain and 27-cm fiber length are the highest yet reported of the SCCFs.

The enhancement mechanism is related to transformation from Cr^{3+}(octa) to Cr^{4+}(tetra) in the chromium-doped fiber under the annealing process. The enhancement mechanism is experimentally confirmed by several measurements with high-resolution transmission electron microscope (HRTEM), X-ray diffraction (XRD), thermal gravimetric analysis (TGA), electron spectroscopy for chemical analysis (ESCA), electron probe X-ray micro-analysis (EPMA), and superconducting quantum interference device (SQUID). For practical application in fiber transmission of the proposed 8-dB gain in the SCCFs, a 25-Gb/s error-floor free data transmission is successfully demonstrated by realizing the high-speed transmission of signal with gain through the SCCFs. This indicates that it is possible to utilize the SCCF as broadband fiber amplifier for use in the next-generation fiber transmission systems.

2. Fabrication

An aligned optimization LHPG system to fabricate the SCCFs was used and integrated with a 60W-CW CO_2 laser heat source, along with few reflective mirrors, two CCDs, a power controller, and a growth chamber [6], [7]. We optimized the molten zone like a trapezoid during the fiber growth process. Fig. 1 shows different shapes of LHPG molten zone. Fig. 1(a) was an ideal trapezoid molten-zone shape, which was used as a reference to align LHPG process. A suitable speed ratio and CO_2 laser power intensity were used to grow the crystal fibers [16]–[18], as shown in Fig. 1(b) of a symmetrical molten-zone shape. However, for asymmetrical molten-zone shapes, such as Fig. 1(c) and 1(d), Fig. 1(a) was used as a reference to re-align during growth process by adjusting the CO_2 laser power intensity. Therefore, the uniform diameter ($<$0.7 μm) with different lengths of the 70-μm and 25-μm diameter single crystal fibers were achieved,

TABLE 1
Different Parameters of Six Fabricated Fibers

Fiber index	I	II	III	IV	V	VI
Core diameter (μm)	70	70	70	70	25	25
Fiber length (cm)	1	1	1	1	27	27
Annealing temperature (°C)	0	900	1000	1100	0	1000
Annealing time (hour)	NA	12	12	12	NA	12
High-index Glass cladding	No	No	No	No	Yes	Yes
Fluorescence improvement	NA	75%	112%	37%	NA	32%

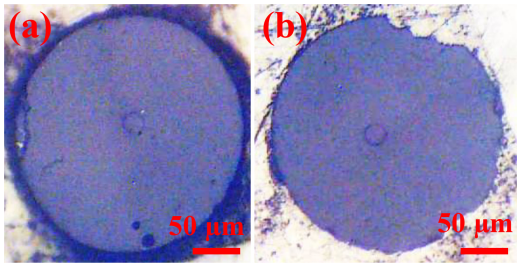

Fig. 2. End-face of 25-μm core diameter of SCCFs (a) without annealing and, (b) with annealing at 1000 °C.

which would be the core material of the SCCFs. Before coating the glass cladding on the single crystal fiber, we would first anneal those 70-μm and 25-μm diameter single crystal fibers. Because the Cr-ion was highly volatile at high temperature and limited to concentration of 0.1 wt%, it was difficult to obtain high-enough Cr^{4+}-ions concentrations [10]. It was reported that the Cr^{4+}-ions was enhanced by thermal annealing [11]–[14]. In this study, the fiber samples were annealed in air environment for 12 hours at different temperatures of 900 °C, 1000 °C, and 1100 °C. Finally, the 25-μm single crystal fibers were tightly-clad with the high-index glass tubes (N-SF57, SCHOTT) to form the SCCFs during high-temperature CO_2 laser fusing. The power of CO_2 laser was well controlled to melt only the high-index glass tube, which softening temperature was 716 °C. The melting temperature of Cr^{4+}:YAG crystal was 1970 °C. Those high-index glass tubes were used to reduce the core/cladding index-different ($<$0.2%) and fabricated by fiber drawing tower with the inner and outer diameters of 90/320 μm. More detailed information of single-mode characteristic of the SCCFs were displayed in Section 3.5. Table 1 lists the different parameters of six fabricated fibers. In this study, the 70-μm core diameter of single crystal fibers were used to verify the material mechanism and optimize the fabricated parameters. The 70-μm fibers were not cladded with the high index glass. The results were applied to develop fiber amplifiers of the SCCFs with 25-μm core diameter. There was no obvious different between the fiber endface images of the SCCFs before and after annealing, as shown in Fig. 2(a) and (b).

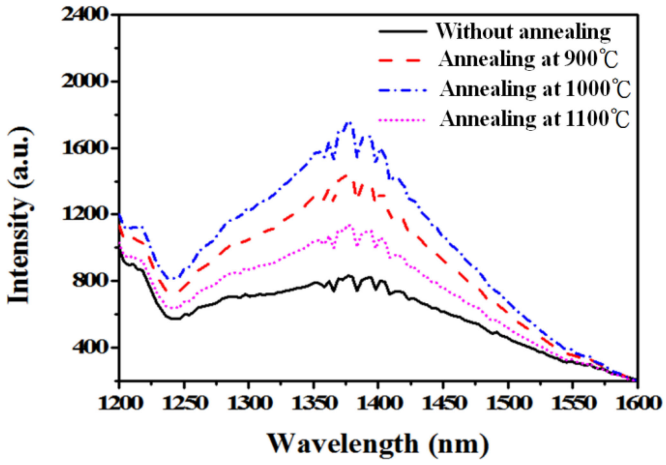

Fig. 3. The fluorescence spectrum of a 70-μm core diameter fiber pumped by $\lambda = 1064$ nm with and without different annealing temperatures.

3. Measurement

3.1 Fluorescence Spectrum Measurement

An Nd:YAG laser source with wavelength of 1.064-μm and pump power of 600 mW was employed for measuring the fluorescence intensity profiles. The 70-μm diameter of the single crystal fibers without annealing and with different annealing temperatures from 900 to 1100 °C were each measured in the same experimental structure by using an optical spectrum analyzer (OSA). The 70-μm single crystal fibers were fabricated with the same fiber length of 1-cm. Fig. 3 shows the fluorescence spectrum as function of wavelengths from 1200 to 1600 nm, which is attributed by Cr^{4+}-ions at tetragonal sites. The fluorescence intensities at 1380 nm wavelength were about 826-, 1435-, 1740-, and 1126-nW/nm for the 70-μm diameter of the single crystal fibers with and without different annealing temperatures, respectively. It indicated that the fluorescence intensity increased as the annealing temperature increased under air environment. The fluorescence intensity of sample III improved 112% compared with sample I without annealing process at the 1380 nm wavelength, as shown in Table 1. However, the fluorescence intensity decreased as the annealing temperature increased to 1100 °C. This was due to the saturation of the fluorescence intensity in the 70-μm single crystal fibers. The trend of the fluorescence spectrum of the 70-μm core diameter was similar to the 25-μm. The Cr^{4+}(tetra) enhanced mechanism of annealing process of chemical shifts might be represented by the two equations as follow [11]–[13]:

$$Cr^{3+}(\text{octa}) + 1/2\,O_2 \rightleftharpoons Cr^{4+}(\text{octa}) + O^{2-} \tag{1}$$

$$Cr^{4+}(\text{octa}) + Al^{3+}(\text{tetra}) \rightleftharpoons Cr^{4+}(\text{tetra}) + Al^{3+}(\text{octa}) \tag{2}$$

Equations (1) and (2) showed that the Cr^{3+}(octa) in the Cr:YAG adsorbed oxygen and transformed into the Cr^{4+}(octa) and then the Cr^{4+}(octa) transformed into the Cr^{4+}(tetra), resulting in the higher fluorescence intensity. Detailed understating of these two equations from the Cr^{3+}(octa) to Cr^{4+}(tetra) was quantitatively investigated by the TGA, ESCA, EPMA, and SQUID measurements in Sections 3.3 and 3.4.

3.2 HRTEM and XRD Measurements

To investigate the crystal structure of the 70-μm single crystal fibers, a HRTEM (JEOL JEM-3010) equipped with a LaB6 electron gun operating at 300 kV was employed. Fig. 4(a) and (c) showed the HRTEM images of a $<111>$ oriented YAG single crystal (a cubic space group is

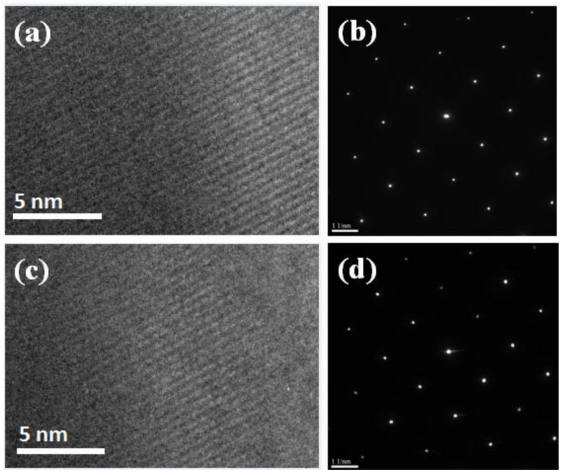

Fig. 4. HRTEM images of single crystal fibers: (a) without annealing, (b) SAED pattern from (a) area, (c) with annealing at 1000 °C, and (d) SAED pattern.

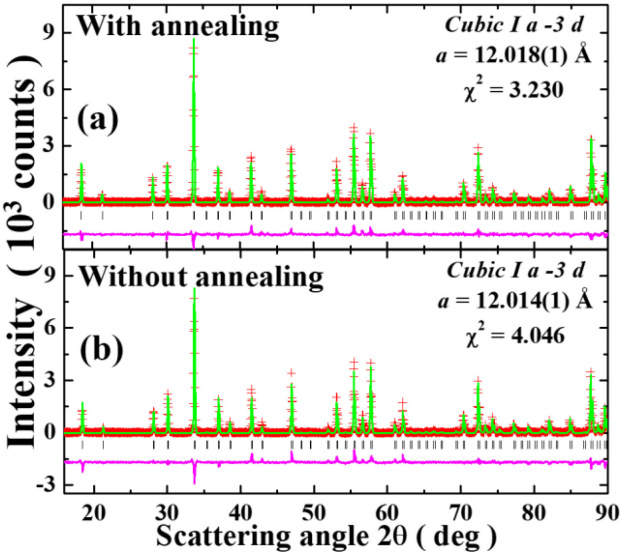

Fig. 5. X-ray diffraction patterns of 70-μm single crystal fibers (a) with and (b) without annealing. The red plus, solid green line, and the magenta line below the short dashes are the observed, calculated, and their difference, respectively. The short dashes are the estimated diffraction peak positions.

Ia3d) with and without annealing at 1000 °C, respectively. The hexagonal sharp bright diffraction spots of the selected area electron diffractions (SEADs) verified the <111> single crystal structure [19], as shown in Fig. 4(b) and (d). An XRD with Bruker D8 diffractometer was also used to determine the crystallographic phase of the 70-μm single crystal fibers. Fig. 5 displays the refined X-ray diffraction patterns of each fiber with and without annealing at 1000 °C. The collected data was analyzed by riveted method with the general structure analysis system (GSAS) program. Two samples were the pure cubic phase and formed in *Ia-3d* space group. No trace of impurity was found within the instrument detection limits. The obtained lattice constants of two samples with and without annealing were 12.018Å and 12.014Å, respectively. This indicated that the effect of uniformity of the fabricated 70-μm single crystal fibers with and without annealing were very small in the X-ray diffraction pattern measurements. The HRTEM images

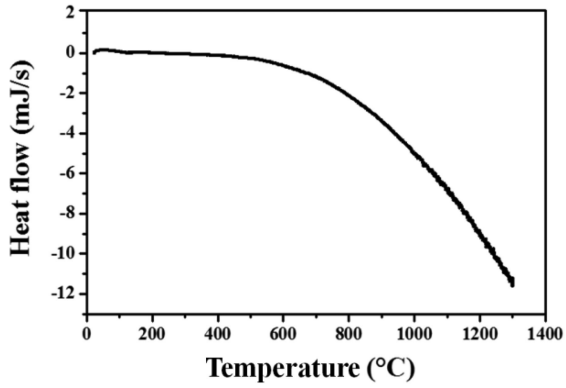

Fig. 6. TGA curve of Cr-doped single crystal powder under air environment.

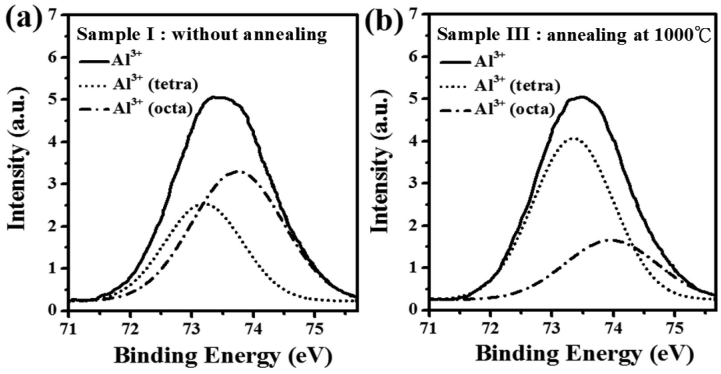

Fig. 7. Al^{3+} binding energy of single crystal powders (a) without annealing and (b) with annealing at 1000 °C.

and XRD results showed that the single crystal structure was still coexisting after the annealing process.

3.3 TGA and ESCA Measurements

To understand the chemical shift of the Cr^{4+}(octa) transforming into the Cr^{4+}(tetra), as indicated in equation (1) and (2), the Thermogravimetric analysis (TGA) and electron spectroscopy for chemical analysis (ESCA) measurements were investigated. A thermal TGA (TGA2950) was analyzed that a 10-mg starting weight of Cr-doped single crystal powder as function of annealing process from 24 °C to 1300 °C under air environment. The experimental temperature ramp was set at 5 °C/min. This measurement provided information about physical phenomena and the chemical shifts of equation (1). Fig. 6 shows dynamic TGA curve of Cr-doped single crystal powder during the annealing process. It indicates that the Cr-doped single crystal of heat flow decreased as temperature increased. The mechanism of Cr^{3+}(octa) transformed into the Cr^{4+}(octa) at the heating temperature higher than 800 °C was due to the Cr^{3+}-ions adsorbing oxygen and then releasing a lot of heat capacity. To prepare the ESCA (ULVAC-PHI), the 70-μm Cr-doped single crystal fibers with and without annealing at 1000 °C were ground into powder. Then those Cr-doped crystal powders were inserted into a capsule to perform the ESCA measurement. Because of the lower concentration ($<$0.1wt%) of Cr-ions, the ESCA measurement cannot directly detect the Cr^{3+}/Cr^{4+}-ions and has the aid of the Al^{3+}-ions. Fig. 7(a) and (b) showed the Al^{3+} binding energy of two powder samples, respectively. We used the Gaussian fitted curves to separate the Al^{3+}(tetra) and Al^{3+}(octa) from Al^{3+}-ions. The two peaks were based on the Gaussian fitting of the binding energy from Al^{3+}(tetra) and Al^{3+}(octa) with 73.2eV and 73.9eV [11], respectively, as shown in the

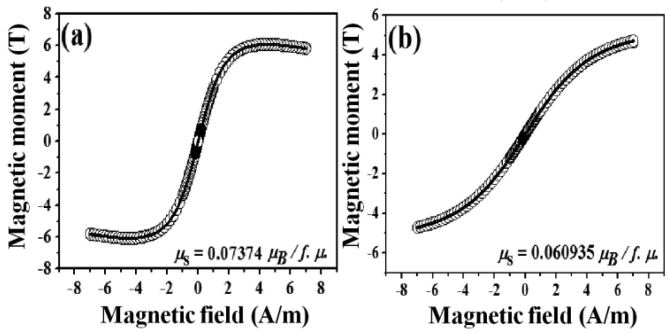

Fig. 8. Hysteresis loops and magnetic moment of single crystal powders (a) without annealing and, (b) with annealing at 1000 °C.

different dashed lines of Fig. 7(a) and (b). The results showed that the number of Al^{3+}/Cr^{3+}(octa) decreased and the number of Al^{3+}/Cr^{4+}(tetra) increased at annealing temperature of 1000 °C under air environment. This was in agreement with the chemical shift in the equation (2).

3.4 SQUID and EPMA Measurements

In order to verify the Cr^{4+} enhanced concentration after annealing process, a superconducting quantum interference device (SQUID, MPMS-3) was a sensitive magnetometer used to measure differently subtle magnetic fields from Cr^{3+}- and Cr^{4+}-ions in the Cr:YAG, which can represent by the Brillouin function and then convert into the concentration ratios between Cr^{3+}- and Cr^{4+}-ion. The Brillouin function could be assumed as follow [20]:

$$M = N\sqrt{x \cdot (3\mu B)^2 + (1-x) \cdot (2\mu B)^2} \tag{3}$$

where the N is the numbers of magnetic ions and the *x* and *(1 − x)* are the concentration ratio of Cr^{3+}- and Cr^{4+}-ion with net magnetic moments (μ_z) of 3 and 2 μB [19], respectively. Fig. 8(a) and (b) show the Hysteresis loops and magnetic moment of the 70-μm single crystal fibers with and without annealing at 1000 °C, respectively, where the $<\mu_z>$ is the projection of average magnetic moment at z-direction (z is the direction of the external applying magnetic field, the unit μB/f.u.). On the basis of the $M = \mu_z = (7.37 \times 10^{-2})$ μB without annealing, $M = \mu_z = (6.09 \times 10^{-2})$ μB with annealing, and equations (3), we could deduce that the concentration ratios of Cr^{4+}-ions increased from 31% to 48%; whereas the Cr^{3+}-ions decreased from 69% to 52% after annealing. The relative concentration of the Cr^{4+}-ions increased about 17% after annealing under air environment. Beside, an electron probe X-ray micro-analysis (EPMA, JXA-8900R) was characterized the chromium concentration in the 70-μm single crystal fibers with and without annealing, as shown in Fig. 9(a). EPMA measurement only can quantitate the concentration of each atom without separating Cr^{3+}/Cr^{4+}-ions. We integrated the SQUID and EPMA results into Fig. 9(b), which showed that the relative weight percentages of total Cr-ion were decreased under annealing. Even though total Cr-ions was volatilized, the weight percentages of the Cr^{3+} and Cr^{4+}-ions were 0.044 wt% and 0.018 wt% without annealing process, respectively. After the 1000 °C annealing process, the weight percentages of the Cr^{3+}- and Cr^{4+}-ion were changed to 0.017 wt% and 0.025 wt%, respectively. Compared with the experimental test results of the TGA, ESCA, SQUID, and EPMA with fluorescence conclusion, it was consistent that the concentration of the Cr^{4+}-ions in the single crystal fibers was enhanced by adopting thermal annealing. Based on the aforesaid results, the 25-μm core diameter and 27-cm fiber length of the SCCFs with and without annealing at 1000 °C were demonstrated the amplifier performance at the next section.

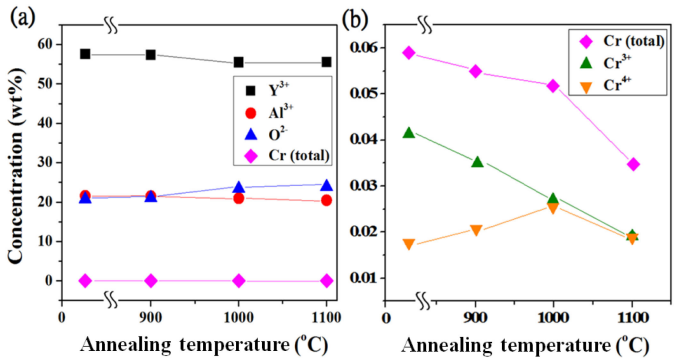

Fig. 9. (a) EPMA of the Cr:YAG with and without various annealing temperatures, (b) enlargement of (a).

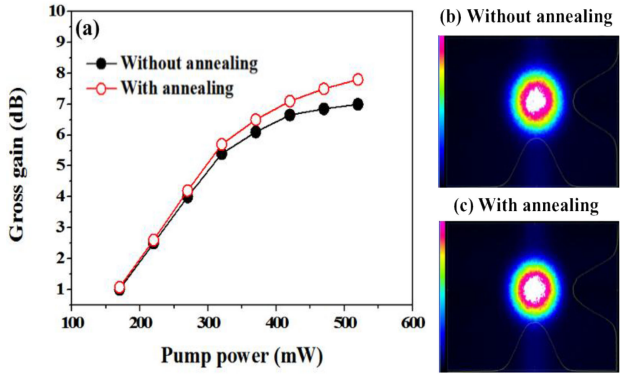

Fig. 10. Gross gain and far field patterns of the SCCFs without and with thermal annealing at 1000 °C.

3.5 Gain and Transmission Performance of the SCCFs

The gross gain performance of the 25-μm core diameter SCCFs were measured by an optical spectrum analyzer with a single pump experimental structure [5]. The 1.4-μm signal source and 1.064-μm pump source were injected into the SCCF through a 2 $\times$ 1 coupler. The gross gain of fiber amplification is defined as G = 10*log [($P_{s+p} - P_p$)/P_s], where the P_s, P_p, and P_{s+p} were the output power from the facet of the SCCF in the operation of injecting only signal beam, only pumping beam, and both input signal and pumping beam, respectively. The gross gain represents a component gain which describes the fiber amplification by optical pumping beam. Fig. 10(a) shows the measured highest gross gains of 7-dB and 8-dB were obtained with and without annealing at 1000 °C, respectively. The measured parameters of the SCCF were a 27-cm fiber length, a 1.30-μW signal power, and a 520-mW pump power. The 14% gain improvement from 7 to 8-dB by annealing was mainly due to the Cr^{4+}(tetra)-ion enhancement in the SCCFs. The gain enhancement mechanism was directly related to the transformation from Cr^{3+}(octa) to Cr^{4+}(tetra) in the core of the SCCF. In fiber amplifier system [9], the net gain represents a gross gain with consideration of insertion loss and is defined as $G_{net} = G_{gross}$ – IL, where the IL is an insertion loss in dB unit and measured the variation between input and output signal power at the facet of SCCF. The insertion loss of 2-dB was achieved by applying a test signal at the input and measuring the power delivered at the output in the absence of the pumping. Therefore, a net gain of 6 dB for a 27-cm-long SCCF with annealing process was obtained at a wavelength of 1.4-μm.

The transmission losses of SCCF included absorption loss of Cr^{4+}-ion, pumping loss, impurity loss, and background loss. The background loss was attributed to both scattering loss and fiber non-uniform loss. The transmission losses of the SCCF were measured by the cutback method,

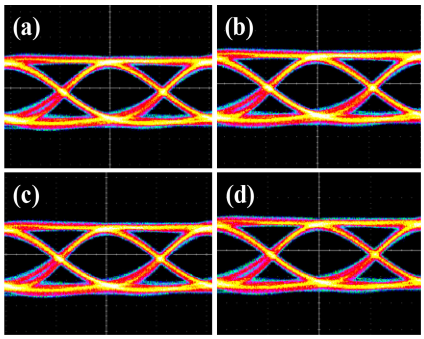

Fig. 11. The measured eye diagrams of SCCF. (a) BTB, (b) no pump, (c) pump 240 mW, and (d) pump 520 mW.

which was similar to the absorption spectra. The measured transmission loss with and without annealing were 0.32 dB/cm and 0.23 dB/cm at the wavelength of 1.4 μm, respectively [7].

For further study of gain improvement, the simulations of the SCCFs were modeled. The gain simulation model of the SCCF was evaluated as the gross gain as function of optimized fiber length, transmission loss, and annealing process. In the simulation of the SCCFs, the background loss of the SCCF with annealing at 1000 °C was about 0.36 dB/cm and the absorption coefficient of the Cr^{4+}-ions was 0.85 cm^{-1} at 1064 nm wavelength [7]. The ground-state absorption and ESA cross section were set as 22 $\times$ 10^{-19} and 7 $\times$ 10^{-20} cm^2, respectively [22]. The lifetime was 3.6 μs at room temperature. The emission cross section at the center wavelength was 3.5 $\times$ 10^{-19} cm^2 [22]. The simulated result indicates that with transmission loss and annealing process a higher gross gain more than 10-dB may be achieved at pump power of 520 mW if a longer fiber length of 40-cm is used. Therefore, further study on higher gain of more than 10-dB gross gain of the SCCFs including a lower loss fiber, a longer length of 40-cm, and a suitable annealing technique may contribute to potential practical fiber amplifier for the next-generation fiber transmission system.

In order to limit the transmitted mode in the fiber core, we choose the high-index glass ($n_{cladding} = 1.826$) as the fiber cladding to match up with the Cr:YAG ($n_{core} = 1.828$) as the core material. Accordingly, the index difference of SCCF was 0.2% at the wavelength of 1.4-μm. Fig. 10(b) and (c) also showed the measured far-field patterns of SCCF with and without annealing at 1000 °C at the propagation wavelength of 1.4-μm. In order to eliminate the cladding effect, macro-bending with the facilitation of index matching gel was employed during measuring process. A single-mode (LP_{01}) characteristic was clearly observed at 1.4-μm wavelength that the most of transmission power intensity was confined in the core of SCCF. For further verifying the *V*-parameter in the SCCFs, the divergence angle of 2.45° and the numerical aperture of 0.0428 were estimated from the far-field pattern measurement [21]. This corresponded to normalized frequency *V*-parameter 2.40 at 1.4-μm and 2.17 at 1.55-μm for single-mode characteristics of SCCF.

For practical application in fiber transmission of the proposed 8-dB gain in the SCCFs, a 25-Gb/s data rate with bit error rate (BER) testing system was employed to investigate the performance of long-haul optical fiber transmission over 30-km. A 1550 nm signal light and a 1064 nm pumping light were adopted in the measurement. A non-return-to-zero (NRZ) electrical 25-Gb/s pseudo random binary sequence with pattern length of $2^{31} - 1$ was generated by pulse pattern generator sending into a Mach Zenhder modulator and then creating 25-Gb/s optical data. After receiving from a high-speed photo-detector to convert electrical signal, the modulated optical data was send into the SCCF for analysis. Eye diagram and BER were obtained from a sampling oscilloscope with an electrical bandwidth of 30 GHz and error detector system, as shown in Fig. 11 and Fig. 12, respectively. There were four testing conditions on the eye diagram and BER measurements: back to back (BTB) without a SCCF, SCCF without pumping, SCCF with 240 mW, and SCCF with 520 mW pumping. Figs. 11(a)–(d) show the measured eye diagrams of SCCF in four different testing conditions. The clear eye openings without waveform distortion were all observed in these

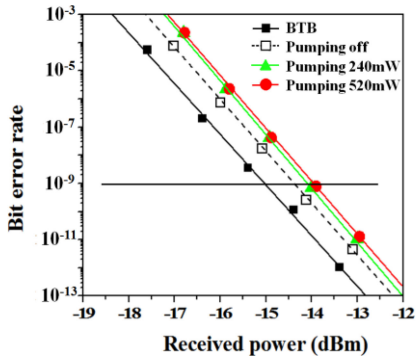

Fig. 12. The measured BERs of SCCFs.

eye patterns. In comparison with back to back (BTB) condition, there was no significant degradation in other three eye patterns. Furthermore, no pattern dependence was observed through the eye diagrams. Fig. 12 shows the BER performances of four testing conditions against received power. This indicated that the obtained power penalties were from 0.8 to 1.2 dB at the BER of 10^{-9} in comparison with the BTB testing condition. All the BER performance showed successful data transmission and exhibited no error-floor. This result further verified that no pattern dependence was observed in the SCCFs.

4. Discussion and Conclusion

In summary, a thermal annealing technique with aligned optimization LHPG was successfully demonstrated for gain enhancement of the broadband SCCFs. The gross gains of 7 and 8-dB for a 27-cm-long fiber of the SCCF with and without annealing at 1000 °C, respectively, were obtained. The 14% gain improvement by annealing was mainly due to the Cr^{4+}(tetra)-ions enhancement in the SCCFs. The 8-dB gross gain and 6-dB net gain were the highest yet reported of the broadband SCCFs. The enhancement mechanism of the Cr^{4+}(tetra)-ions in the fiber was experimentally verified by the means of TGA, ESCA, EPMA, and SQUID. With the help of an optical-fiber system examination for the SCCF, a 25-Gb/s error-floor free data transmission was displayed by realizing the high-speed transmission of signal with gain through the SCCFs. The result may indicate that it is possible to utilize the SCCF as a broadband fiber amplifier for use in the next-generation fiber transmission systems.

The Cr^{4+}(tetra)-ions were the major factor to provide gain in the broadband SCCFs. The net gain and pump to signal conversion efficiency of the SCCF amplifier were still low, as shown in Fig. 10. Because of the Cr^{4+}-ions in the SCCFs were significantly reduced and difficult to maintain high-enough Cr^{4+}-ions during high-temperature LHPG multi-growth [10], resulting in limited Cr^{4+}-ions to provide higher gain of the SCCFs. Further gain improvement by developing higher Cr^{4+}-ions is the main factor in the SCCFs. However, in this work, the highest Cr doping concentration in a 1-mm-thick of Cr:YAG rod was not more than 0.1 wt%. Furthermore, the EPMA result showed that the Cr doping concentration of a 25-μm core of the Cr:YAG was reduced to about half of 0.059 wt% after high-temperature LHPG multi-growth. Therefore, further gain improvement by developing low loss fiber, long fiber length, and high weight percentage of the bulk Cr:YAG using dielectric coating, such as Cr_2O_3 and CaO coatings on the surface of the Cr:YAG and then the Cr^{4+}-ions enhancement in the Cr:YAG employing annealing technique are essential and are currently under investigation.

Acknowledgment

The authors would like to thank Prof. Charles Tu, Prof. Silvano Donati, and Prof. Nan-Kuang Chen for helpful suggestion on the manuscript.

References

[1] T. Kasamatsu, Y. Yano, and H. Sekita, "1.50-μm-band gain-shifted thulium-doped fiber amplifier with 1.05- and 1.56-μm dual-wavelength pumping," *Opt. Lett.*, vol. 24, no. 23, pp. 1684–1686, Dec. 1999.

[2] Y. Ohishi, T. Kanamori, T. Kitagawa, S. Takahashi, E. Snitzer, and G. H. Sigel, "Pr^{3+}-doped fluoride fiber amplifier operating at 1.31 μm," *Opt. Lett.*, vol. 16, no. 22, pp. 1747–1749, Nov. 1991.

[3] I. A. Bufetov *et al.*, "Bi-doped optical fibers and fiber lasers," *IEEE J. Sel. Top. Quant. Electron.*, vol. 20, no. 5, Oct. 2014, Art. no. 0903815.

[4] S.V. Firstov *et al.*, "A 23-dB bismuth-doped optical fiber amplifier for a 1700-nm band," *Sci. Rep.*, vol. 6, Jun. 2016, Art. no. 28939.

[5] W. L. Wang *et al.*, "Single-mode Cr-doped crystalline core fibers for broadband fiber amplifiers," *IEEE Photon. Technol. Lett.*, vol. 27, no. 2, pp. 205–208, Jan. 2015.

[6] C. N. Liu, G. L. Cheng, N. K. Chen, P. L. Huang, S. L. Huang, and W. H. Cheng, "Gain enhancement of single-mode Cr-doped core fibers by online growth system," *IEEE Photon. Technol. Lett.*, vol. 28, no. 19, pp. 2098–2101, Oct. 2016.

[7] C. N. Liu, T. H. Wang, T. S. Rou, N. K. Chen, S. L. Huang, and W. H. Cheng, "Higher gain of single-mode Cr-doped fibers employing optimized molten-zone growth," *J. Lightw. Technol.*, vol. 35, no. 22, pp. 4930–4936, Nov. 2017.

[8] B. M. Tissue, W. Jia, L. Lu, and W. M. Yen, "Coloration of chromium-doped yttrium aluminum garnet single-crystal fibers using a divalent codopant," *J. Appl. Phys.*, vol. 70, pp. 3775–3777, Oct. 1991.

[9] S. M. Yeh *et al.*, "Broadband chromium-doped fiber amplifiers for next-generation optical communication systems," *J. Lightw. Technol.*, vol. 30, no. 6, pp. 921–927, Mar. 2012.

[10] K. P. Lillerud and P. Kofstad, "On high temperature oxidation of chromium," *J. Electrochem. Soc.*, vol. 127, no. 11, pp. 2397–2410, 1980.

[11] C. N. Tsai *et al.*, "Distribution of oxidation states of Cr ions in Ca or Ca/Mg co-doped Cr:$Y_3Al_5O_{12}$ single-crystal fibers with nitrogen or oxygen annealing environments," *J. Cry. Growth*, vol. 310, no. 11, pp. 2774–2779, May 2008.

[12] R. Feldman, Y. Shimony, and Z. Burshtein, "Dynamics of chromium ion valence transformations in Cr, Ca:YAG crystals used as laser gain and passive Q-switching media," *Opt. Mater.*, vol. 24, no. 1–2, pp. 333–344, Nov. 2003.

[13] A. Sugimoto, Y. Nobe, and K. Yamagishi, "Crystal growth and optical characterization of Cr,Ca: $Y_3A_{l5}O_{12}$," *J. Cry. Growth*, vol. 140, no. 3-4, pp. 349–354, May 2008.

[14] Y. C. Huang *et al.*, "Fluorescence enhancement in broadband Cr-doped fibers fabricated by drawing tower," *Opt. Exp.*, vol. 21, no. 4, pp. 4790–4795, 2013.

[15] C. N. Liu, J. W. Li, C. C. Yang, C. Tu, and W. H. Cheng, "Higher-gain of broadband single-mode chromium-doped fiber amplifiers by tetrahedral-chromium enhancement," in *Proc. Opt. Fiber Commun. Conf. Exhib.*, San Diego, CA, USA, Mar. 3-7, 2019.

[16] R. S. Feigelson, "Pulling optical fibers," *J. Cryst. Growth*, vol. 79, no. 1-3, part 2, pp. 669–680, Dec. 1986.

[17] C. Y. Lo and P. Y. Chen, "Three-dimensional simulation and experiment on micro-floating zone of LHPG with asymmetrical perturbation," *J. Cryst. Growth*, vol. 362, pp. 45–51, Jan. 2013.

[18] A. Yariv and P. Yeh, *Photonics: Optical Electronics in Modern Communications*, 6th ed., Oxford U. Press, 2006.

[19] B. M. Tissue, W. Jia, L. Lu, and W. M. Yen, "Coloration of chromium-doped yttrium aluminum garnet single-crystal fibers using a divalent codopant," *J. Appl. Phys.*, vol. 70, pp. 3775–3777, Oct. 1991.

[20] Y. H. Tung, C. C. Yang, T. W. Hsu, C. W. Kao, and Y. Y. Chen, "Size effects on magnetic property of multiferroic $DyMn_2O_5$ nanorods," *AIP Advances*, vol. 7, no. 7, Mar. 2017, Art. no. 055830.

[21] Y. Shamir, Y. Sintov, E. Shafir, and M. Shtaif, "Beam quality output of a few-modes fiber seeded by an off-center single-mode fiber source," *Opt. Lett.*, vol. 34, no. 12, pp. 1795–1797, Jun. 2009.

[22] G. Xiao, J. H. Lim, S. Yang, E. V. Stryland, M. Bass, and L. Weichman, "Z-scan measurement of the ground and excited state absorption cross sections of Cr^{4+} in yttrium aluminum garnet," *IEEE J. Quantum Electron.*, vol. 35, no. 7, pp. 1086–1091, Jul. 1999.